

UCAV model design and static experimental investigations to estimate control device effectiveness and Stability and Control capabilities

Kerstin C. Huber¹

German Aerospace Center (DLR), Braunschweig, Germany

Dan D. Vicroy²

NASA Langley Research Center, Hampton, VA, USA

Andreas Schütte³

German Aerospace Center (DLR), Braunschweig, Germany

Andreas-René Hübner⁴

German-Dutch Wind Tunnels, Braunschweig, Germany

The experimental investigations of two generic UCAV configurations with control surfaces are presented. The current paper is covering the design of the model, layout of the control surfaces as well as the static wind tunnel tests. The low speed static wind tunnel tests have been undertaken to evaluate the effectiveness of different control surfaces and control surface settings. Finally, the experimental results are used to establish a common CFD test matrix for the NATO STO Task Group AVT-201 for computer code validation and to assess the capability to predict the complex vortical flow and aerodynamic Stability and Control (S&C) characteristics of configurations with highly swept leading edges and vortex dominated flow field.

Nomenclature

α	=	AoA, Angle of attack [°]	$S\&C$	=	Stability and Control
β	=	AoS, Angle of side slip [°]	TE	=	Trailing Edge
η	=	Flap deflection angle [°]	c_r	=	Length of root chord [m]
Θ	=	Pitch angle [°]	C_{ref}	=	Reference length [m]
Ψ	=	Yaw angle [°]	C_L	=	Lift coefficient (AE) [-] $L/(q_\infty \cdot A)$
V_∞	=	Free stream velocity [ms^{-1}]	C_D	=	Drag coefficient (AE) [-] $D/(q_\infty \cdot A)$
A	=	Reference relation area [m^2]	C_Y	=	Side force coefficient (AE) [-] $S/(q_\infty \cdot A)$
AE	=	Aerodynamic Coordinate System	C_m	=	Pitch moment coefficient (AE) [-] $M/(q_\infty \cdot A \cdot C_{ref})$
AVT	=	Applied Vehicle Technology	C_l	=	Roll moment coefficient (AE) [-] $l/(q_\infty \cdot A \cdot s)$
$CFRP$	=	Carbon Fiber Reinforced Plastic	C_n	=	Yaw moment coefficient (AE) [-] $n/(q_\infty \cdot A \cdot s)$
CS	=	Control Surface	c_p	=	Pressure coefficient [-] $p-p_\infty/q_\infty$
DoF	=	Degree of Freedom	x	=	Chord wise coordinate [m]

¹Research Engineer, DLR Institute of Aerodynamics and Flow Technology, Lilienthalplatz 7, 38108 Braunschweig, Germany.

²Senior Research Engineer, Flight Dynamics Branch, MS 308, NASA LaRC, Hampton, VA 23681, AIAA Associate Fellow.

³Research Engineer, DLR Institute of Aerodynamics and Flow Technology, Lilienthalplatz 7, 38108 Braunschweig, Germany, AIAA Senior Member.

⁴Deputy Head of the Low Speed Wind Tunnel Braunschweig (DNW-NWB), Lilienthalplatz 7, 38108 Braunschweig, Germany.

<i>HLP</i>	=	Hinge Line Position
<i>l</i>	=	Rolling Moment [Nm]
<i>LE</i>	=	Leading Edge
<i>LIB</i>	=	Left Inboard
<i>LOB</i>	=	Left Outboard
<i>M</i>	=	Pitch moment [Nm]
<i>MPM</i>	=	Model Positioning Mechanism
<i>Ma</i>	=	Mach Number [-]
<i>MRP</i>	=	Moment Reference Point
<i>n</i>	=	Yaw moment [Nm]
<i>PIV</i>	=	Particle Image Velocimetry
<i>Re</i>	=	Reynolds Number [-]
<i>RIB</i>	=	Right Inboard
<i>RLE</i>	=	Round Leading Edge
<i>FT</i>	=	Fixed Transition
<i>ROB</i>	=	Right Outboard
<i>RPM</i>	=	Revolution per Minute
<i>S</i>	=	Sideforce [N]
<i>SACCON</i>	=	Stability and Control Configuration
<i>STO</i>	=	Science and Technology Organization

<i>y</i>	=	Span wise coordinate [m]
<i>p</i>	=	Local pressure [Nm ⁻²]
<i>p_∞</i>	=	Free stream pressure [Nm ⁻²]
<i>s</i>	=	Half span [m]
<i>q_∞</i>	=	Dynamic pressure [Nm ⁻²] $0.5 \cdot \rho_{\infty} \cdot V_{\infty}^2$
<i>z</i>	=	Vertical coordinate [m]

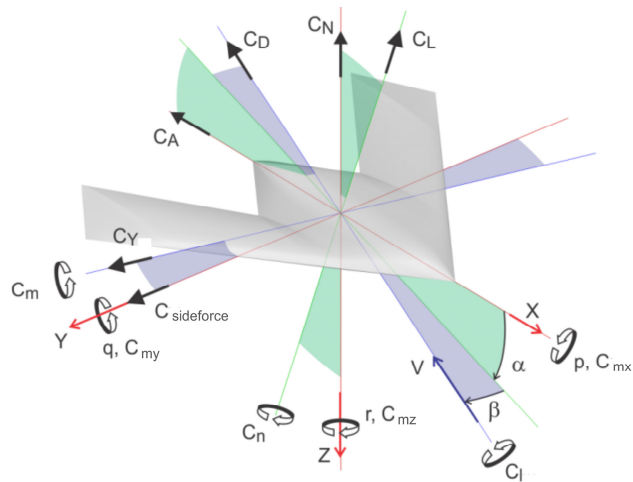


Figure 1 Coordinate axes convention for the DLR-F19.

I. Introduction

As part of an internal DLR Project and the international NATO task group STO AVT-201 (Extended Assessment of Reliable Stability & Control Prediction Methods for NATO Air Vehicles), three wind tunnel experiments have been conducted. Within three wind tunnel experiments (T0, T1 and T2) with the SACCON were conducted whereas during an additional wind tunnel campaign (T3) the DLR-F19 was in focus of the experimental investigation. The SACCON was already part of a number of experimental investigations without control surfaces; in depth information can be found among others in Huebner et al.¹. For the planned research within the international NATO/STO AVT-201 research group the SACCON was equipped with static control surfaces on the left hand side of the configuration. A new wind tunnel model DLR-F19 was designed and built within the DLR internal project. This wind tunnel model can be equipped with a range of interchangeable trailing edge control devices. A selected set of experimental results was made available within a common test case matrix of the AVT-201 task group. This report covers the experiments undertaken within the test campaigns in the German-Dutch wind tunnels DNW low speed atmospheric wind tunnel Braunschweig (DNW-NWB). The campaigns took place between 2011 and 2013. The static tests include α - and β -sweeps. During the dynamic tests the model was subjected to forced sinusoidal oscillations in the modes of pitch and yaw as described in Vicroy et al.². The wind tunnel models have been suspended from the Model Positioning Mechanism (MPM) during the entire measurement campaigns. The main objective of the three test campaigns was to assess the influence of different flap settings, applied to both, the left hand and the right hand side of the model, on the aerodynamic properties and the flight mechanical behavior of the configuration at speeds of $V_{\infty} = 50 \text{ ms}^{-1}$, corresponding to $Ma = 0.15$. Also high speed wind tunnel experiments have been conducted, which are described in detail in Irving et al.³. The plan form of the two wind tunnel models is the same and hence it is possible to conduct reproducibility tests to not only show reproducibility within the current tests but also between model configurations and wind tunnel setup.

II. The SACCON and the DLR-F19 Wind Tunnel Models

Within this chapter the model layout of the SACCON and the DLR-F19 is drawn out. These two wind tunnel models are identical in their plan form. The SACCON was built at NASA Langley Research Center (LaRC) and the data was evaluated in the NATO AVT-161/201 task groups. Further information on the SACCON can be found in Cummings and Schuette.^{4,5} The DLR-F19 is the successor model of the SACCON. The model DLR-F19 was designed and built at DLR Research Center in Braunschweig.

Figure 1 illustrates the coordinate axes convention as it will be used throughout this work. This coordinate system is the same as applied within Vicroy et al.² and Liersch and Huber.⁶

A. SACCON

The SACCON (Stability and Control Configuration) is a generic UCAV model. It is the predecessor model for the DLR-F19. The basic design of the SACCON was developed within the NATO STO/AVT-161 task group. The manufacturing and engineering was under the responsibility of NASA at NASA Langley Research Center (LaRC).

The plan form is of lambda wing type. It has a leading edge sweep angle of 53° . The model has a wing span of $b = 1.54$ m, a root chord of $c_r = 1.06$ m and a wing area of $S = 0.77$ m². A plan form drawing including all dimensions is given in **Figure 2**.

An overview of the work which was and will be undertaken is described in Cummings and Schuette.⁷ Further information on the flow characteristics around the configuration using experimental data and numerical calculations with the SACCON without control surfaces can be found in Loeser et al.,⁸ Vicroy et al.,⁹ Schuette et al.¹⁰ and Huber.¹¹

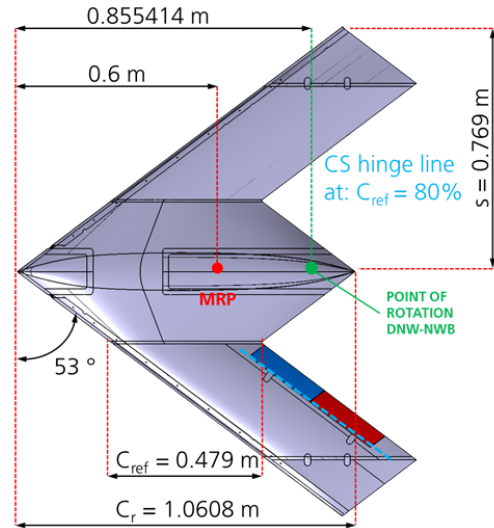


Figure 2 Model layout of the SACCON with control surfaces on the left hand side of the configuration only.

B. DLR-F19

The second model used within this set of experiments is the DLR-F19 model. The model is dimensioned for static as well as dynamic testing, up to a maximum velocity of $V_\infty = 90$ ms⁻¹ ($Ma = 0.256$). The model has a weight of approximately 10 kg and is of modular set-up, i.e. control surfaces can easily be exchanged and refitted. The control surfaces are not movable, hence for each angle of deflection a specific control surface exists. In **Table 3** all control surfaces used during the wind tunnel test T3 are listed.

The differences between the DLR-F19 configuration and the SACCON configuration, which has been tested in the DNW-NWB during various test campaigns, are the following:

- Control surface depth can be varied between 20% up to 30% reference chord length, i.e. the hinge line location can be varied between $70\% \leq C_{ref} \leq 80\%$.
- Control surfaces are located on the LHS and RHS side of the configuration, as well as on the wing tips, as seen in **Figure 3** above.

The model is equipped with a fixed transition by means of fine corundum grit particles. A removable latex based paint was used to fix the transition and hence it is possible to remove and reapply fixed transition without harming the surface of the wind tunnel model. This set up can be seen in **Figure 4** and **Figure 5**. The area of fixed transition of the DLR-F19 is the same as it has been applied for the SACCON model considered within Vicroy et al.⁹

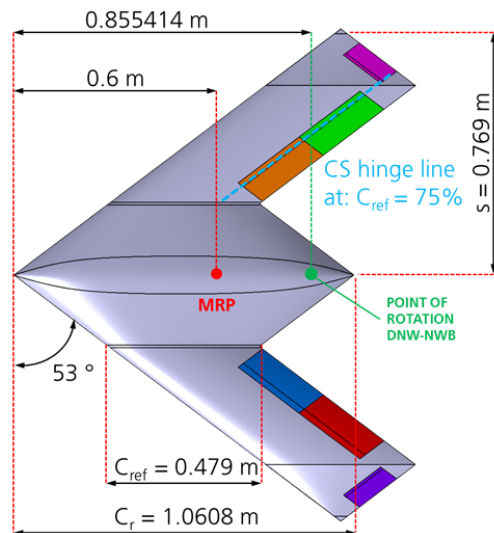


Figure 3 Model layout of the DLR-F19 configuration and its control surfaces.

C. Control Deflection Options

The SACCON was originally built without control surfaces. However during its conceptual design stage the possibility of equipping the models left hand side with control surfaces at a later stage was given. The authors would like to call attention to the fact that the wind tunnel models are hung upside-down in the wind tunnel. In Figure 4 the location and sign convention of the control surfaces for the two wind tunnel models is shown. The control surfaces of the SACCON are located within the red box. The control surfaces of the DLR-F19 can be seen clearly within the lighter regions of the wind tunnel model.

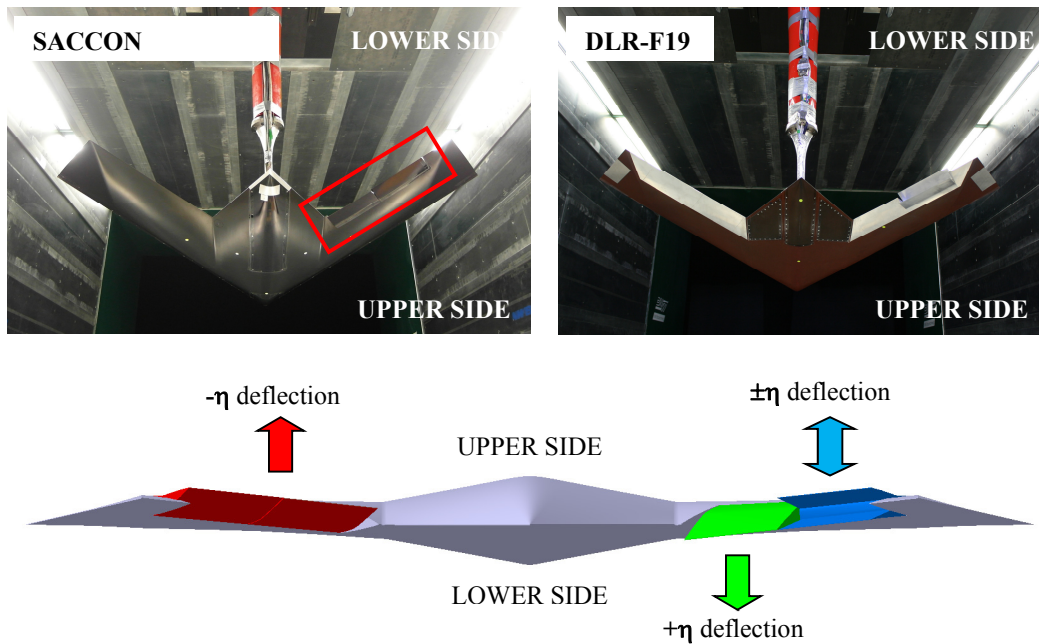


Figure 4 Model layout of the SACCON with control surfaces and the DLR-F19 configuration followed by an illustration of the sign convention.

Within Table 1, Table 2 and Table 3, all possible surface deflection configurations considered during the three test campaigns considering control surface deflections are listed. T0 is a wind tunnel experiment where only the baseline configuration without any control surfaces and control surface deflection has been considered. The results from T0 serve also as base for reproducibility and repeatability. During Test T1 with the SACCON model only single deflections on the left hand side of the configuration were considered. During Test T2 with the SACCON model combined deflections were considered. Finally during Test T3 using the DLR-F19 model single and combined control surface deflections on both wings of the configuration have been considered.

T1 SACCON	Deflections					
		LOB	LIB			
RLE_FT_IB00_OB00_SP00	-	-	-	-	-	-
RLE_FT_IB00_OB-5_SP00	-	↑	-	-	-	-
RLE_FT_IB00_OB+10_SP00	-	↓	-	-	-	-
RLE_FT_IB00_OB00_SP20	-	↕	-	-	-	-
RLE_FT_IB00_OB00_SP10	-	↕	-	-	-	-
RLE_FT_IB00_OB00_SP05	-	↕	-	-	-	-
RLE_FT_IB20_OB00_SP00	-	-	↓	-	-	-
RLE_FT_IB10_OB00_SP00	-	-	↓	-	-	-
RLE_FT_IB05_OB00_SP00	-	-	↓	-	-	-
RLE_FT_IB-10_OB00_SP00	-	-	↑	-	-	-
RLE_FT_IB-20_OB00_SP00	-	-	↑	-	-	-

Table 1 : Control surfaces considered within T1 (SACCON single control surface deflections).

T2 SACCON	Deflections					
		LOB	LIB			
RLE_FT_IB00_OB00_SP00	-	-	-	-	-	-
RLE_FT_IB-20_OB00_SP00	-	↑	-	-	-	-
RLE_FT_IB00_OB00_SP20	-	-	↕	-	-	-
RLE_FT_IB-20_OB10_SP00	-	↑	↓	-	-	-
RLE_FT_IB20_OB10_SP00	-	↓	↓	-	-	-
RLE_FT_IB10_OB10_SP00	-	↓	↓	-	-	-
RLE_FT_IB-20_OB-5_SP00	-	↑	↑	-	-	-
RLE_FT_IB20_OB-5_SP00	-	↓	↑	-	-	-
RLE_FT_IB-10_OB-5_SP00	-	↑	↑	-	-	-
RLE_FT_IB10_OB-5_SP00	-	↓	↑	-	-	-
RLE_FT_IB10_OB00_SP20	-	↓	↕	-	-	-
RLE_FT_IB-10_OB00_SP20	-	↑	↕	-	-	-
RLE_FT_IB-20_OB00_SP20	-	↑	↕	-	-	-

Table 2 : Control surfaces considered within T2 (SACCON combined control surface deflections).

T3 DLR-F19	Deflections					
	LTIP	LOB	LIB	RIB	ROB	RTIP
FT_ALL_CS_00	-	-	-	-	-	-
FT_LOB+20_20pct (20%)	-	↕	-	-	-	-
FT_LOB+20 (25%)	-	↕	-	-	-	-
FT_LIB-20 (25%)	-	-	↑	-	-	-
FT_LTIP+20 (25%)	↕	-	-	-	-	-
FT_LTIP+20_LOB+20_LIB-20 (25%)	↕	↕	↑	↓	-	-
FT_LOB+20_LIB-20_RIB+20_ROB+20 (25%)	-	↕	↑	↓	↓	-
FT_RIB+20_ROB+20 (25%)	-	-	-	↓	↓	-
FT_LIB-20_RIB+20 (25%)	-	-	↑	↓	-	-
FT_LOB-20_LIB-20_RIB+20_ROB+20 (25%)	-	↑	↑	↓	↓	-
FT_LOB-20_ROB+20 (25%)	-	↑	-	-	↓	-
FT_RIB+20 (25%)	-	-	-	↓	-	-
FT_LOB-20_LIB-20 (25%)	-	↑	↑	-	-	-
NT_ALL_CS_00	-	-	-	-	-	-
NT_LOB-20_LIB-20_RIB+20_ROB+20 (25%)	-	↑	↑	↓	↓	-

Table 3 : Control surfaces considered within T3 (DLR-F19).

III. Test Set-Up

Within this chapter the test setup is drawn out. Information on the testing facilities will be given. Further the measurement equipment will be explained in more detail.

A. The Low Speed Wind Tunnel Facility DNW-NWB

The DNW-NWB is located on the premises of the DLR in Braunschweig. This wind tunnel is a closed circuit low speed wind tunnel of atmospheric type. The DNW-NWB wind tunnel is used for testing in the low speed domain with capabilities for aero-acoustic, aerodynamic static, dynamic and maneuver testing. The wind tunnel is operated by the foundation German-Dutch Wind Tunnels (DNW). The main characteristics of the DNW-NWB are listed in **Table 4**. Further information with regards to the DNW-NWB and its measurement techniques can be found in on the website of the DNW-NWB¹² and in Bergmann et al.¹³

Test Section used:	closed (static and dynamic tests), slotted, open
Test Section width:	3.25 m
Test Section height:	2.8 m
Test Section area:	9.1m ²
Contraction Ratio S_{sc}/S_N:	5.6
Maximum Velocity:	$0 \leq V_\infty \leq 90\text{m/s}$ ($0 \leq \text{Ma} \leq 0.27$), closed
Fan Power P_{max}:	3500 kW @ 520 RPM

Table 4 : Wind tunnel characteristics of the DNW-NWB.

B. Model Positioning and Mounting Arrangement and Instrumentation

During all measurement runs, static, dynamic as well as maneuver simulations, the model was suspended by a belly sting from the 6-DOF platform MPM. The MPM features struts which are of constant length and are driven by 6 linear electromagnetic motors. There exists an additional actuator on the movable Stewart platform, an electric motor, being part of the MPM, in order to induce a pitching or rolling oscillation motion on the model by means of a pushrod setup. More information on the MPM can be found in Bergmann¹⁴. The following pictures show the models attached to the belly yaw link support with a crank angle of 15°. In all test campaigns in the DNW-NWB, the models were equipped with an internal 6-component strain gauge balance of type Emmen-196-6 in order to gather the forces and moments data.

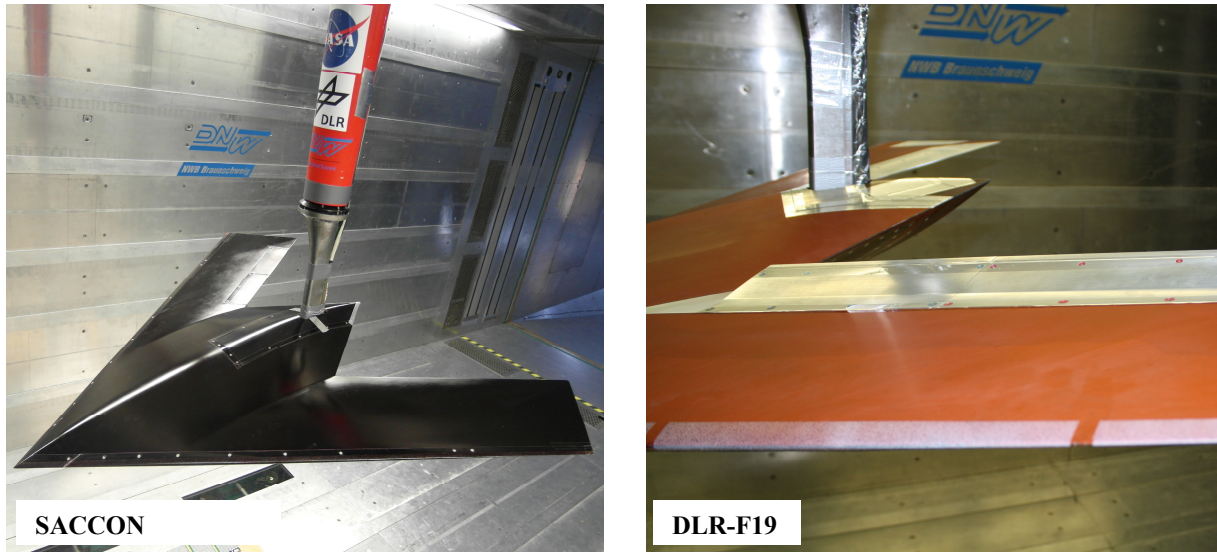


Figure 5 The SACCON and the DLR-F19 configuration wind tunnel model suspended in the DNW-NWB.

Both models have surface pressure cuts, which are illustrated in **Figure 6**. Additionally to the surface pressure stations there are a number of dynamic pressure transducers located over the surface. Hereby it is possible to collect flow field information and the location and development of the vortices over the surface. An evaluation of the flow structure over the DLR-F19 configuration will be discussed in detail in Schuette et al.¹⁵

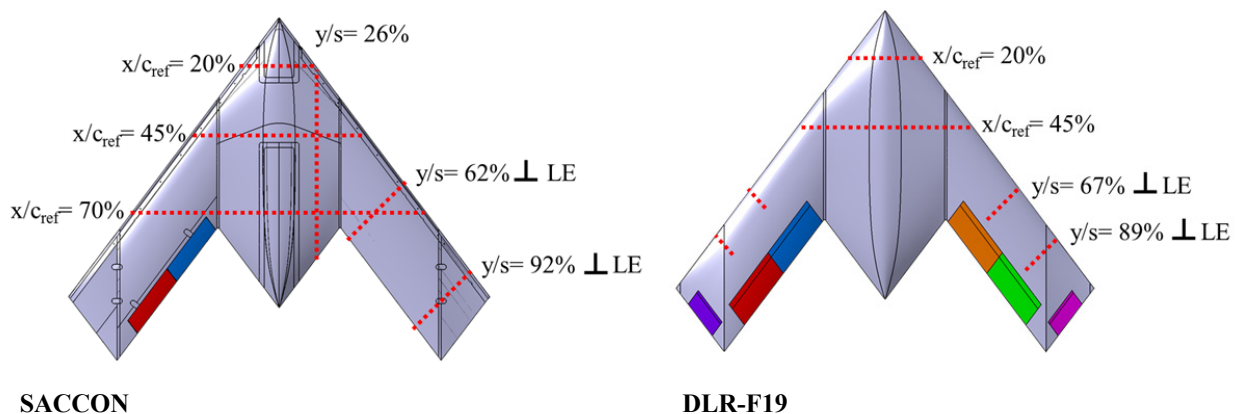


Figure 6 Surface pressure cuts and their location over the SACCON and DLR-F19 configuration.

IV. Results and Discussion

Within this chapter the experimental outcomes will be presented and discussed. First, a representation of the repeatability and hysteresis effects will be given. Then a series of control surface deflection effects will be drawn out and discussed. The results section will be rounded off giving an illustration of superposition effects of single and combined control surface deflections.

A. Repeatability and Reproducibility

1. Alpha Sweep of the Baseline Configuration

As already mentioned in the introduction, these kinds of configurations have limitations in Stability and Control. Hence extensive experimental measurements are conducted in order to create a database for further numerical investigations as well as to model the Stability and Control characteristics. This database is made up of different test results in different wind tunnels with different wind tunnel models which are described in detail in Vicroy et al.⁹ Hereby it is important so show the repeatability and reproducibility between tests and wind tunnel models in order to be able to integrate all experimental investigations into one aerodynamics flight model to undertake Stability and Control analyses, please also refer to chapter “I. Utilization of Experimental Data” at the end of this work.

Figure 7 illustrates the baseline configuration (BL) alpha sweep results at $\beta = 0^\circ$ for all wind tunnel tests undertaken within the low-speed wind tunnel DNW-NWB in Braunschweig, for both model configurations the SACCON and the DLR-F19.

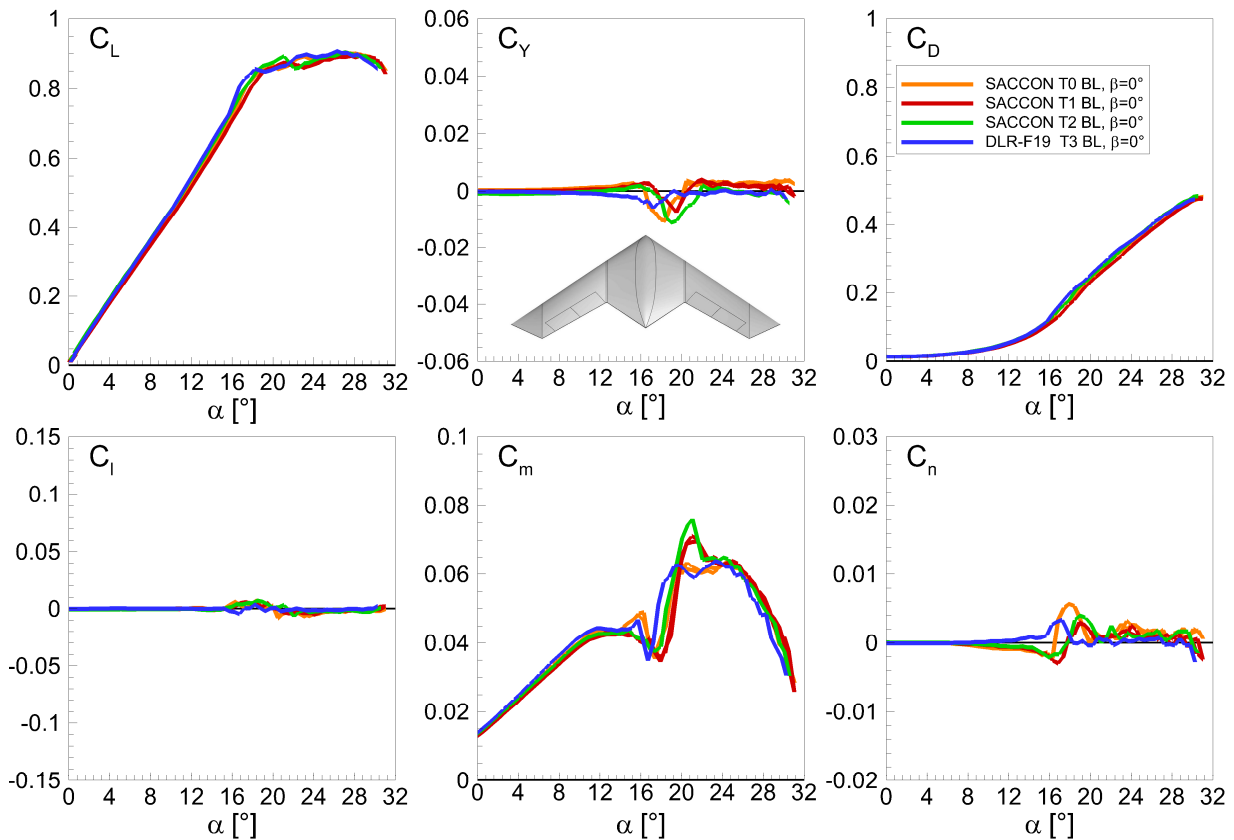


Figure 7 Repeatability and reproducibility between wind tunnel campaigns and different wind tunnel models, α -sweep, baseline configuration all control surfaces at $\eta=0^\circ$.

It can be seen that the repeatability and reproducibility for all forces and moments between angles of attack $\alpha = 0^\circ$ and $\alpha = 15^\circ$ is very good. The repeatability and reproducibility between the lift-, drag- and rolling moment coefficients is very satisfactory for the whole angle of attack range up to an angle of attack of $\alpha = 32^\circ$. Small differences in the curves can be noted for the side force-, pitching- and yawing moment coefficient. The orange curve (T0) and the blue curve (T3), representing the original SACCON without control surfaces and the DLR-F19

respectively, follow the same trend as do the red and green curves representing the results for the SACCON configuration within the test campaigns T1 and T2. The differences between the different tests appear due to the subsequent application of control surfaces to the SACCON configuration. The largest differences occur from an angle of attack $\alpha = 16^\circ$ onwards, where the flow is dominated by strong vortex-to-vortex and vortex-to-surface interactions. These differences are however small and can hence be disregarded for further investigations.

2. Alpha Sweep for Control Surface Deflection $\text{LOB} \pm 20^\circ$:

In order to assure repeatability and reproducibility with deflected control surfaces, alpha sweeps have been conducted with a control surface deflection of $\eta = \pm 20^\circ$ on the left hand outboard control surfaces at $\beta = 0^\circ$. These results are depicted in **Figure 8**. There is a good correlation between all curves. The repeatability for the SACCON during different experimental test campaigns, T1 and T2, is very good. There seems to be distinct differences between the reproducibility experiments conducted with the SACCON (red and green curve) and the DLR-F19 (blue curve), however if the total scale of the yawing moment is considered, the differences between the curves can be neglected.

Hence it can also be shown that the repeatability and reproducibility of results for configurations with control surface deflections is satisfactory.

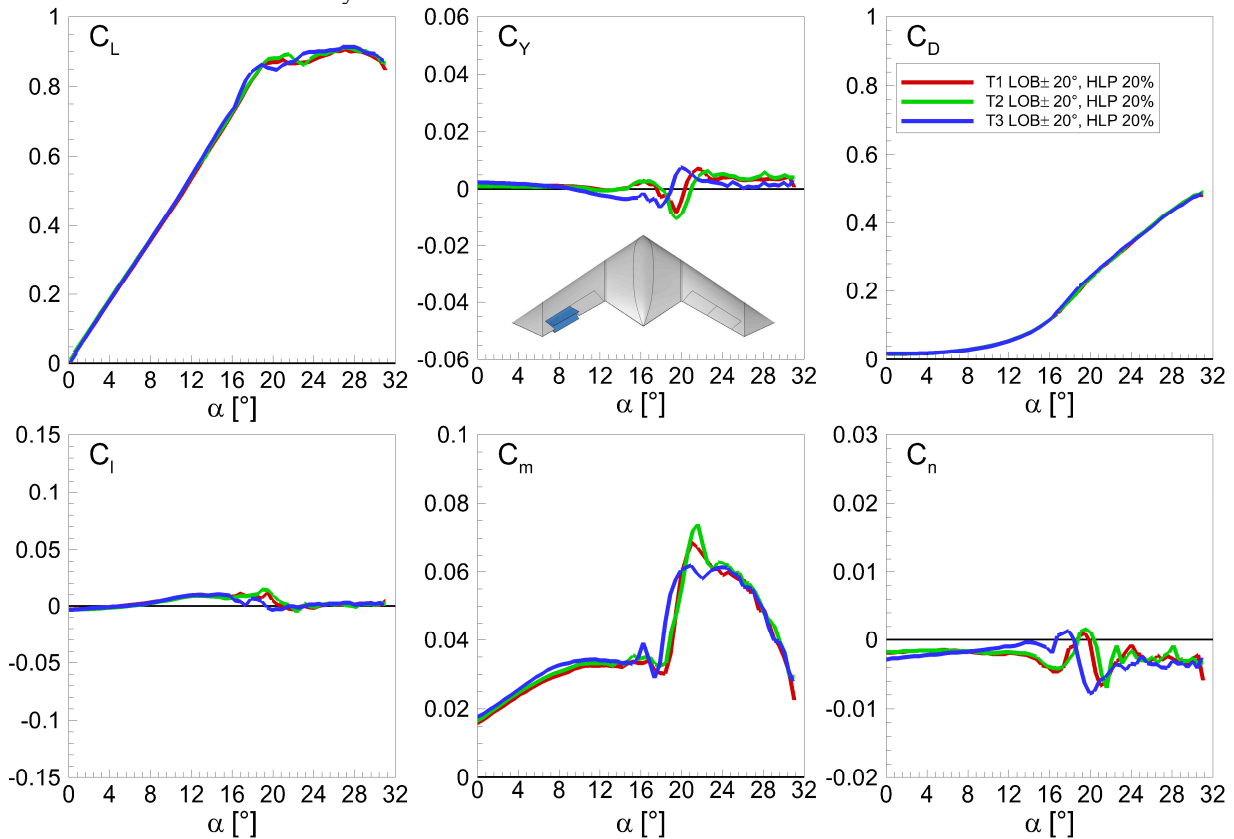


Figure 8 Repeatability and reproducibility between wind tunnel campaigns and different wind tunnel models, α -sweep, control surfaces at $\eta = \pm 20^\circ$ left hand side only.

Concluding it can be said that the repeatability and reproducibility is satisfactory and all experimental investigations of the configuration can be included into further discussion.

B. Effect of Deflection Angle

Figure 9 depicts the effect of deflection angle on the forces and moments coefficient of the SACCON with downward control surface deflections varying from $\eta = 0^\circ$ up to $\eta = 20^\circ$.

The overall effect of the deflection angles of $\eta = 5^\circ$ and $\eta = 10^\circ$ is small. For further Stability and Control investigations distinct differences during control surface deflections are needed in order to identify the different aerodynamic characteristics and effects. For surface control deflections of $\eta = 20^\circ$ larger differences in moment can be noticed. Hence it was decided to use a minimum deflection angle of $\eta = 20^\circ$ for further experimental and numerical investigations with the DLR-F19 configuration.

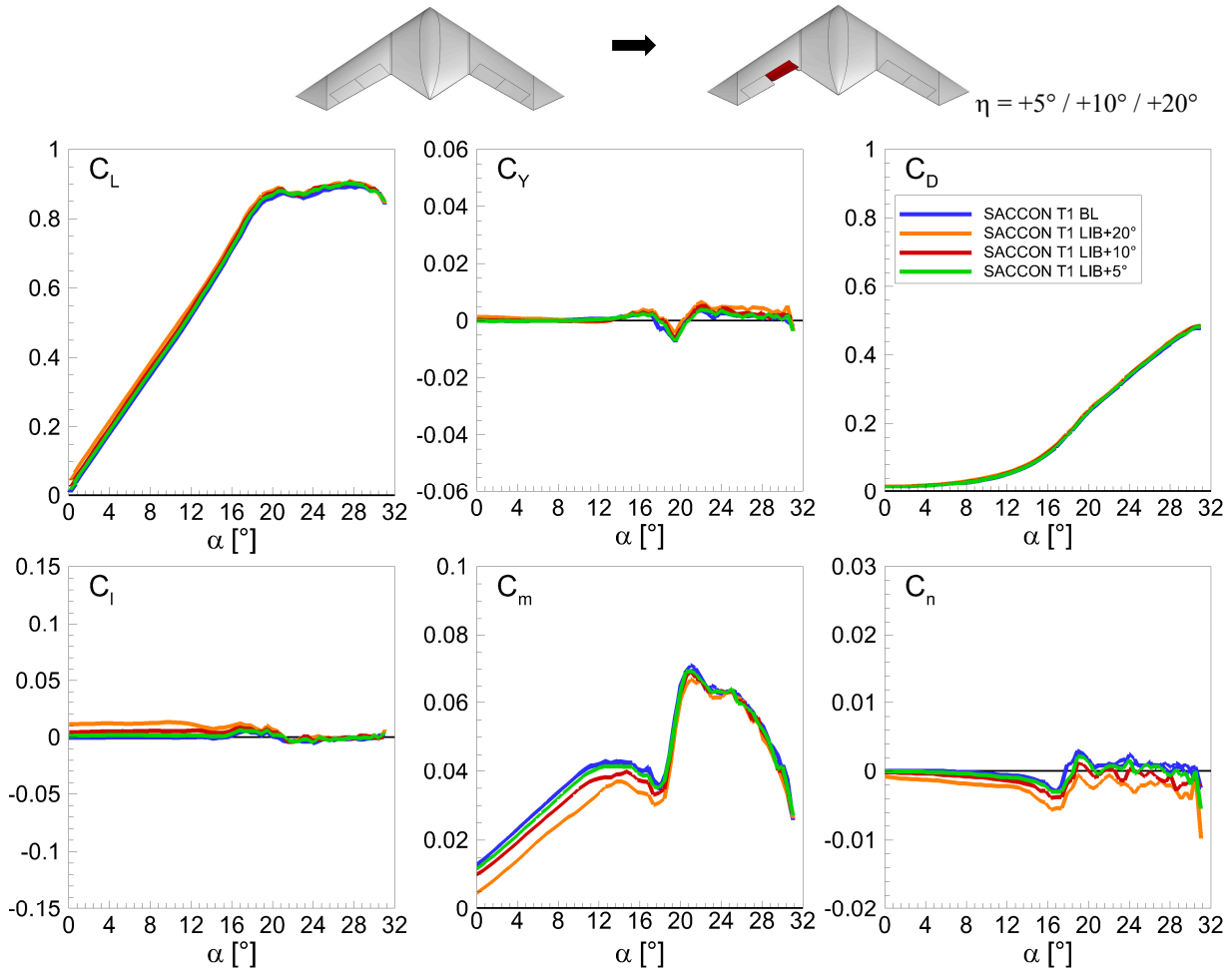


Figure 9 Effect of deflection angle on the forces and moments of the SACCON at $\eta = 0^\circ / +5^\circ / +10^\circ / +20^\circ$, left hand side only.

C. Effect of Control Surface Depth

During the experimental investigations not only the deflection angle effect was studied but also the effect of hinge line position, i.e. control surface depth. **Figure 10** shows the effect of hinge line position on the forces and moments of the DLR-F19 configuration. When considering the lift and drag coefficient no change in coefficient value can be noted. There is a slight difference in side force coefficient value; however this difference value is so small that it can be regarded as being zero. When considering the moment coefficients, it can be seen that the two control surface configurations have very similar moment characteristics. The pitching moment coefficient shows a slight change within the angle of attack range of $\alpha = 8^\circ$ - 10° . The larger control surface depth also seems to introduce a higher, though still relatively small, negative yawing moment.

Overall it can be noticed that the 5% increase in control surface depth has no significant effect on the forces and moments of the configuration. A hinge line position of 75% of C_{ref} was chosen for further experimental investigations.

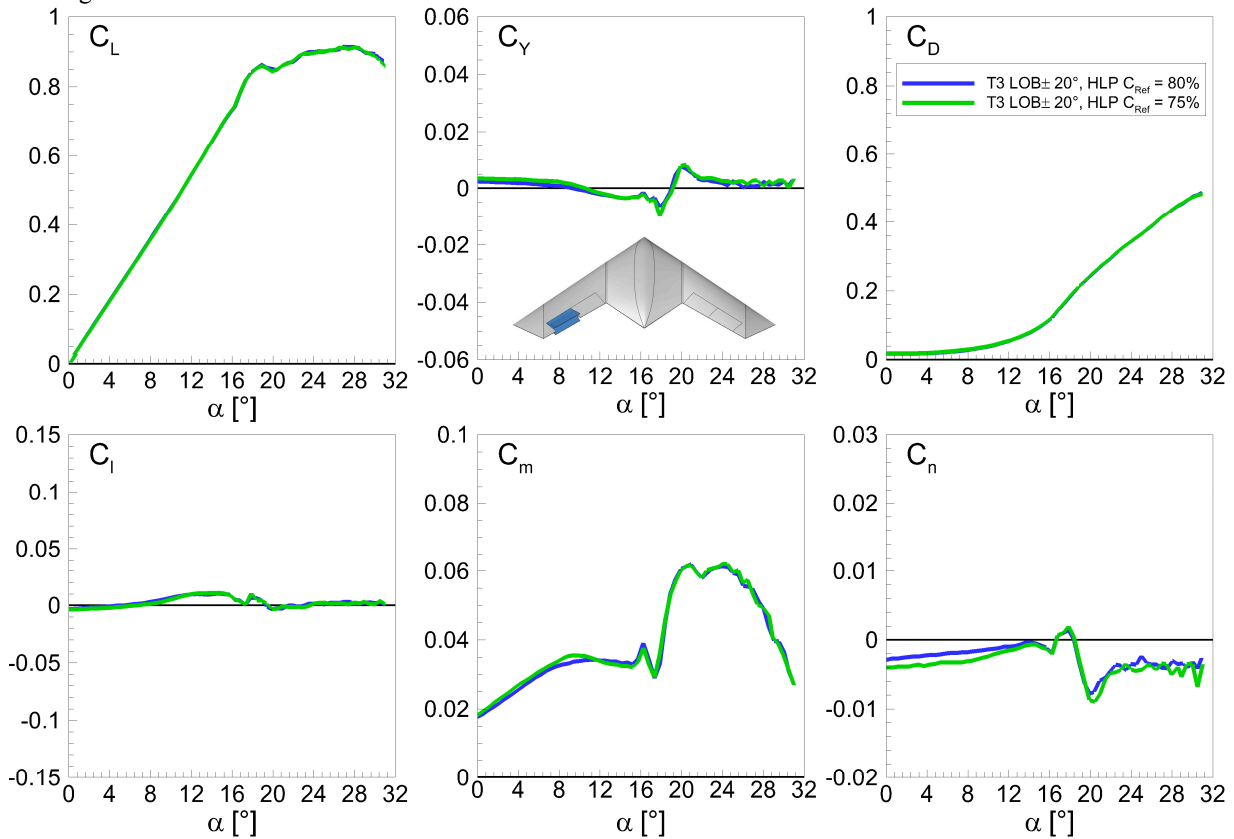


Figure 10 Effect of control surface depth for the DLR-F19 configuration at hinge line positions of 75% of C_{ref} and 80% and a deflection angle of $\eta = \pm 20^\circ$ left hand side only.

D. Effect of Positive Control Surface Deflection

Within this subchapter the effect of positive, downward, control surface deflections will be discussed using the forces and moment curves depicted in **Figure 11**. In order to identify the pure effect due to positive control surface deflection it was chosen to deflect only control surfaces along the right hand side of the configuration.

The right hand side control surfaces are deflected at a hinge line position of 75% of C_{ref} with a deflection angle $\eta = +20^\circ$.

The downward deflection results in a slight increase in lift and drag force and shifts the entire curves upwards. The resulting side force effects are negligible. More distinct effects however can be noted in the moment coefficient curves.

When considering the rolling moment C_l in **Figure 11**, it can be seen that the configuration experiences a negative rolling moment when control surfaces on the right hand side are deflected downwards. The negative rolling moment is created as the right hand side of the configuration experiences an increase in lift due to the downward deflection of the control surfaces. The negative rolling moment increases even further when additionally the outboard control surface is deflected. The increase in negative rolling moment due to the additional deflection of the right outboard control surface of the configuration is little compared to the single deflection effect of the inboard control surface.

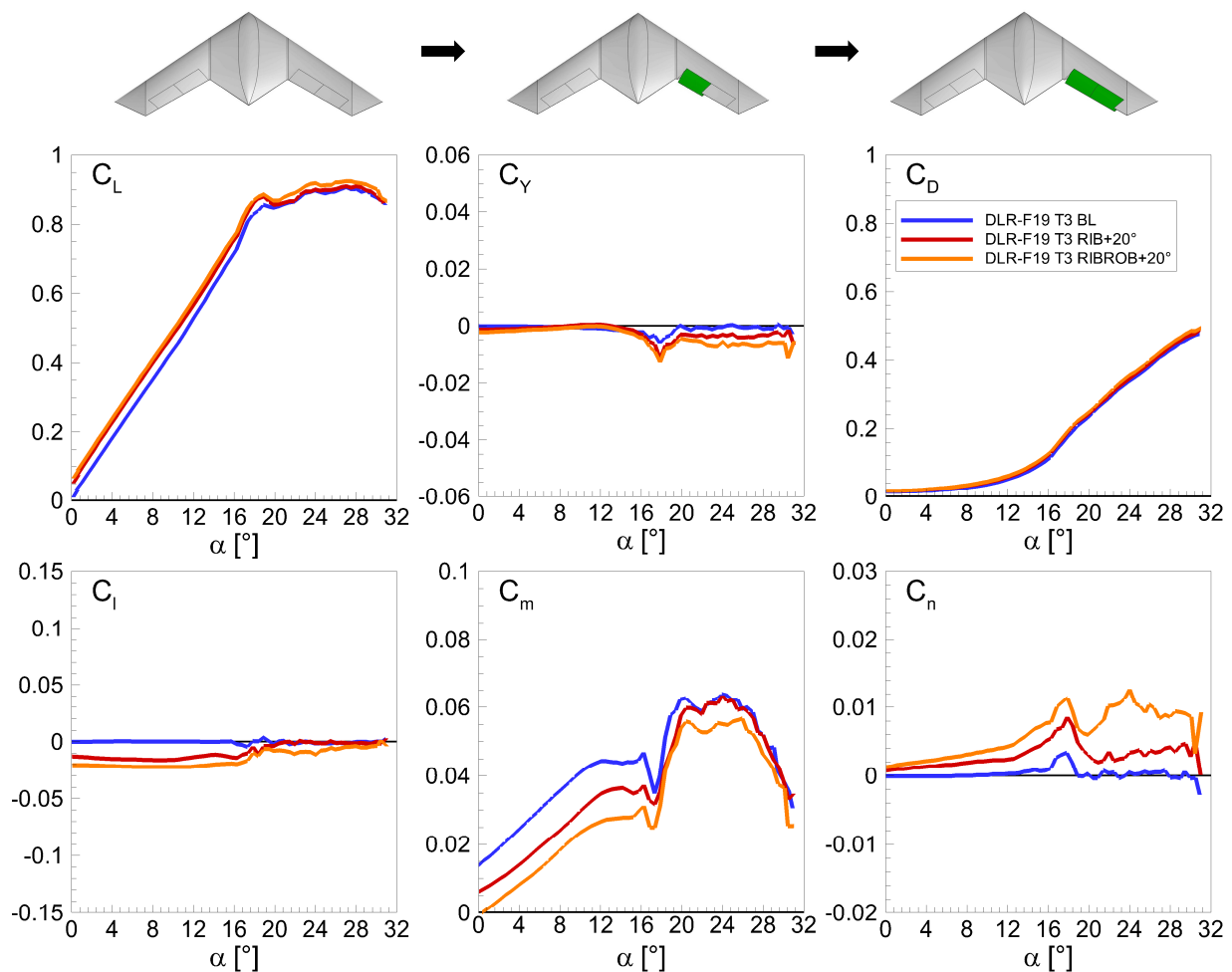


Figure 11 Effect of positive, downwards, control surface deflection on the forces and moment coefficients of the DLR-F19 configuration.

This indicates that the effect of the inboard deflection has a larger influence on the aerodynamic behavior than the effect generated by deflecting the outboard control surface. This assumption is strengthened by the fact that the inboard control surface experiences healthy incident flow orthogonal to its surface compared to the outboard control surface¹⁵. The outboard control surface is exposed to diverted incident flow due to the double vortex structure over the configuration, and hence the influence of the control surface deflection is weakened.

The pitching moment coefficient curve also shows distinct differences in moment behavior. The nose up pitching moment is reduced when deflecting the control surfaces downward. The deflection seems to have a strong effect on the vortex systems, which give the moment coefficient curve its characteristic shape. Detailed information on this topic can be found in Huber et al.¹⁶ and Schuette et al.¹⁵. The deflection seems to destabilize the apex vortex which is the main driver for the pitching moment and seems also to destabilize and weaken the tip vortex. The effect of weakened tip vortex is also indicated by the smaller dip within the moment pitching coefficient curve.

Main aim for these kinds of tailless configurations is to generate a yawing moment which is large enough to control the vehicle. When looking at the yawing moment coefficient curve in **Figure 11** above. The influence of the large positive control surface deflection is still very small. A clear need is given to undertake more investigations to find possible solutions for this drawback.

E. Effect of Negative Control Surface Deflection

Within this subchapter the effect of negative, upward, control surface deflections will be discussed using the forces and moment curves depicted in **Figure 12**. In order to identify the pure effect due to negative control surface deflection it was chosen to only deflect control surfaces along the left hand side trailing edge of the configuration. The left hand side control surfaces are deflected at a hinge line position of 75% of C_{ref} with a deflection angle $\eta = -20^\circ$.

The upward deflection results in a slight decrease in lift the entire curve downward. The resulting side force coefficient and drag coefficient effects are very small and hence negligible. More distinct effects however can again be noted in the moment coefficient curves, as already seen in the previous subchapter. When considering the rolling moment C_l in **Figure 12**, it can be seen that the configuration experiences a negative rolling moment when control surfaces on the left hand side are deflected upwards. The aerodynamic behavior of the configuration with negative control surface deflection is comparable to the aerodynamic behavior of the configuration with positive control surface deflection.

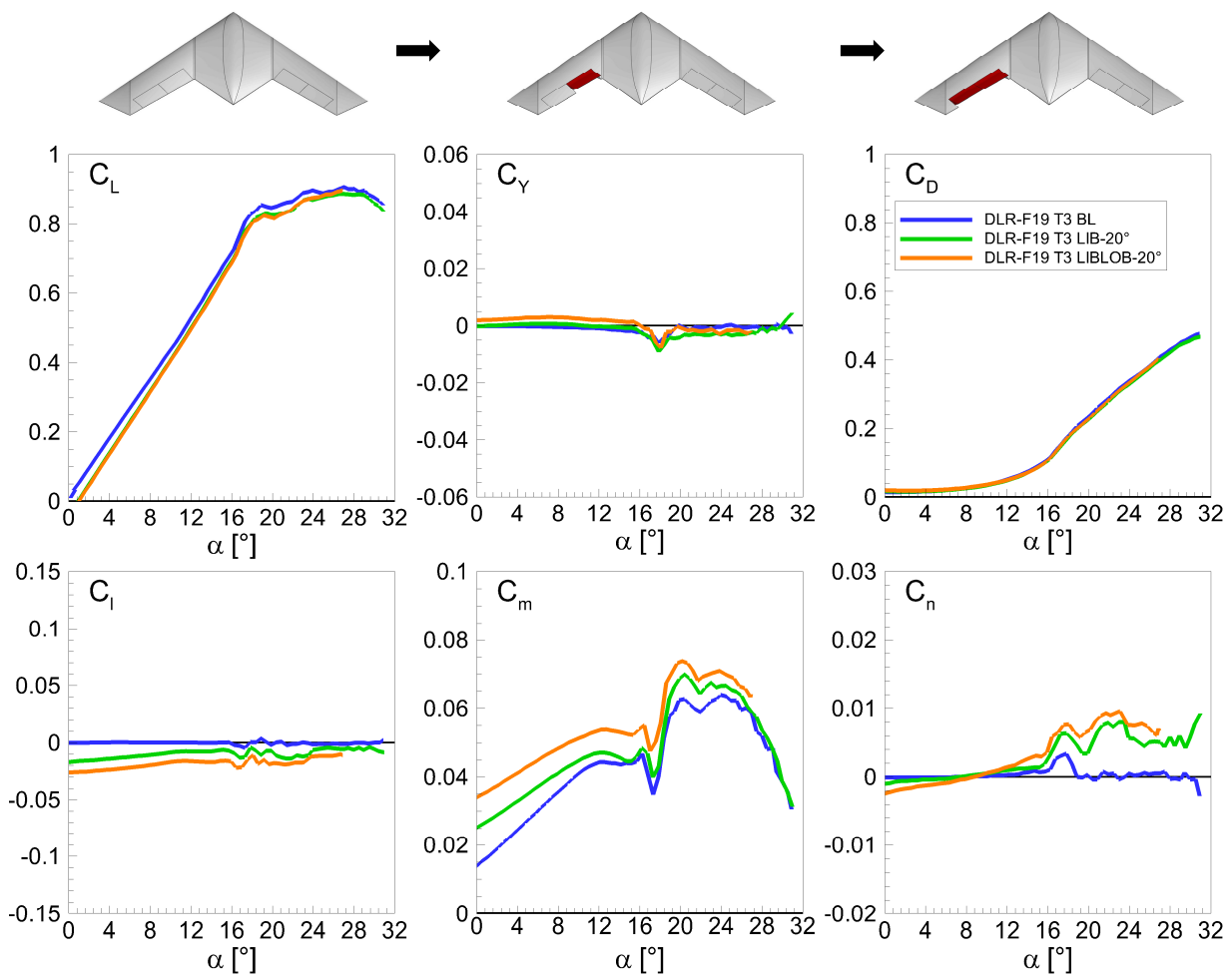


Figure 12 Effect of negative, upwards, control surface deflection on the forces and moment coefficients of the DLR-F19 configuration.

The negative rolling moment however is generated by a different mechanism than was described in the previous chapter. The upward deflection of the control surfaces on the left hand side weakens the vortices such that the left hand side loses lift and the lift value generated by the zero deflection on the right hand side is larger. Hence a negative rolling moment is created. The negative rolling moment increases even further when additionally the outboard control surface is deflected. The increase in negative rolling moment due to the additional deflection of the

right outboard control surface of the configuration is little compared to the single deflection effect of the inboard control surface, as seen also in the previous chapter.

This effect reinforces the assumption even further that the effect of the inboard deflection has a larger influence on the aerodynamic behavior than the effect generated by deflecting the outboard control surface. This effect can again be described such that the inboard control surface experiences healthy incident flow orthogonal to its surface compared to the outboard control surface.

The pitching moment coefficient curve also shows distinct differences in moment behavior. The nose up pitching moment is increased when deflecting the control surfaces upward. When looking at the yawing moment coefficient curve in **Figure 11** above. The influence of the large negative control surface deflection is still very small.

F. Superposition Effects – Inboard Control Surface Deflection

Part of the here presented work is also dedicated to point out possible superposition effects of different control surface deflection combinations. The work aims to answer, if it is possible to add up single deflection effects in order to reproduce the results for the combined control surface deflections. Three cases have been chosen in order to show possible superposition effects.

The first case discusses the effects of one sided single deflected inboard control surface superposition effects as illustrated in **Figure 13**.

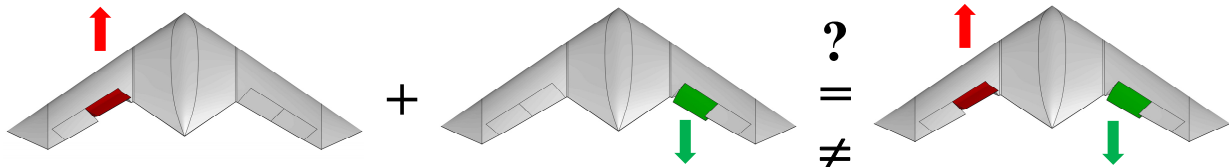


Figure 13 Control surface deflection superposition – inboard control surfaces.

The investigation depicted in **Figure 14** shows the delta effects of the single deflections of RIB+20° (green curve), of LIB-20° (red curve) and of the combined deflection of LIB-20°RIB+20° (black curve). The delta force and moment coefficients are generated by subtracting the baseline configuration from the deflected cases.

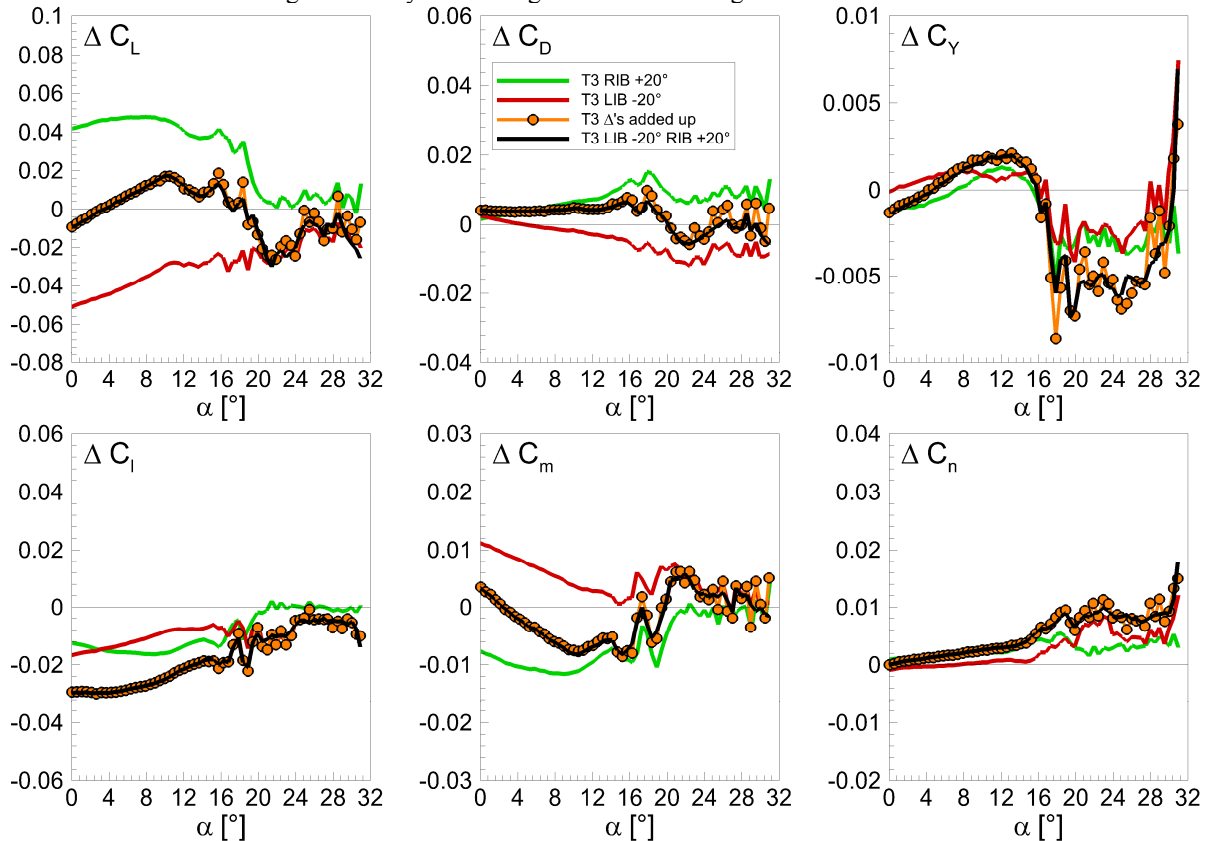


Figure 14 Superposition Effects – inboard control surface deflection.

The orange curve with circular symbols represents the aerodynamic behavior of the configuration of the delta changes of the single deflections are added up. When comparing the results for the combined deflection from the experiment and the superposed results it can be seen that the two curves match very well over the entire angle of attack range tested. Hence it can be shown that the forces and moment coefficients for single deflections can be added up in order to represent the overall behavior of the configuration throughout the entire angle of attack range tested. The match even captures the nonlinearities at higher angle of attack.

This finding has a great influence on the creation of possible Stability and Control databases for this kind of configurations. Delta changes of single deflections on one or the other side of the wing can be added up in order to reproduce the behavior of the combined control surface deflection configuration. This way data bases can be filled with extra points without extra measurements.

G. Superposition Effects – Inboard and Outboard Control Surface Deflection

The second case discusses the effects of the single deflected inboard and single deflected outboard control surface superposition effects as illustrated in **Figure 15**.

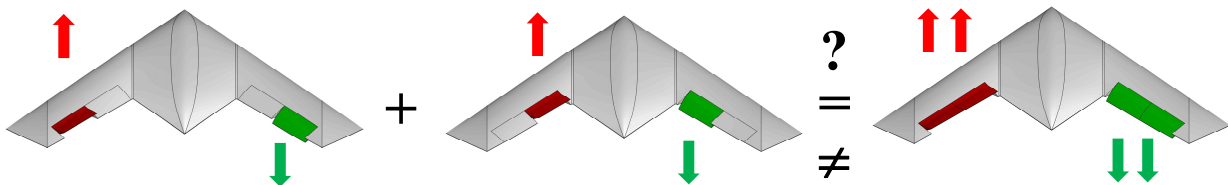


Figure 15 Control surface deflection combinations – inboard and outboard control surfaces.

The investigation depicted in **Figure 16** shows the delta effects of the deflections of LOB-20°ROB+20° (magenta curve), of LIB-20°RIB+20° (blue curve) and of the combined deflection of LIBLOB-20°RIBROB+20° (black curve).

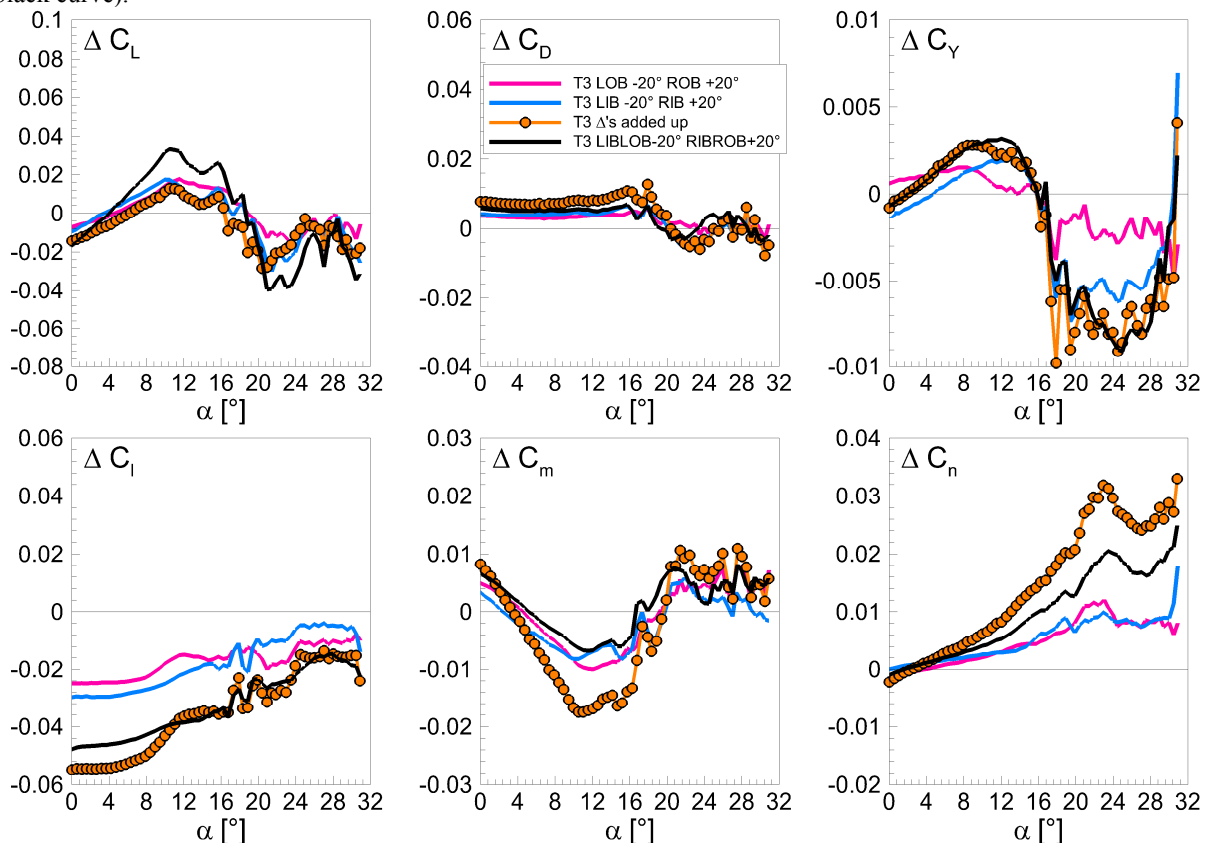


Figure 16 Superposition Effects – inboard and outboard control surface deflection.

When considering the drag and side force coefficient it can be noted that the differences from the experiment and the superposition do match, even for higher angles of attack. The rolling moment coefficient results by the superposition approach over predict the negative rolling moment up to an angle of attack of $\alpha = 12^\circ$, at higher angle of attack the two results match quite well. For the lift, the pitching moment and yawing moment coefficient there are large differences between the experimental and superposed results. The experimental results for LIBLOB-

$20^\circ\text{RIBROB}+20^\circ$ indicate a higher lift increase than the single deflected cases added up. The pitching moment for the $\text{LIBLOB-}20^\circ\text{RIBROB}+20^\circ$ case is smaller than the rolling moments generated by the $\text{LOB-}20^\circ\text{ROB}+20^\circ$ and the $\text{LIB-}20^\circ\text{RIB}+20^\circ$ deflection configuration. Hence the superposed results predict a higher pitching moment decrease than the experimental results. The increase in yawing moment is also over predicted by the superposed result compared to the experimental result for $\text{LIBLOB-}20^\circ\text{RIBROB}+20^\circ$.

Hence it can be shown that the forces and moment coefficients for deflection combinations depicted in **Figure 15** cannot be added up in order to represent the overall behavior of the configuration throughout the entire angle of attack range tested. The control surfaces do influence each other and the effects from the resulting flow mechanisms cannot be added up.

H. Superposition Effects – Full Span Control Surface Deflection

As discussed in the subchapters before, the coefficient changes of single one sided deflection can be added up, the coefficient changes of combined single deflection on the left and right hand side of the configuration cannot be added up to represent the aerodynamic behavior from the experiment. The third case discusses the effects of full span deflection superposition effects as illustrated in **Figure 17**.

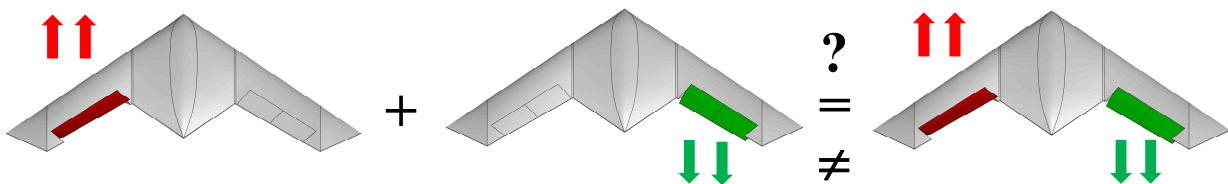


Figure 17 Control surface deflection combinations – full span control surface deflection.

The investigation depicted in **Figure 18** shows the delta effects of the deflections of $\text{LIBLOB-}20^\circ$ (red curve), of $\text{RIBROB}+20^\circ$ (green curve) and of the combined deflection of $\text{LIBLOB-}20^\circ\text{RIBROB}+20^\circ$ (black curve).

When considering the delta change of force coefficients for lift, drag and side force it can be noted that the results from the experiment and the results from the superposition do not match throughout the entire angle of attack range tested. Although the superposition results for the lift coefficient over predict the change in lift coefficient within the experiments, it follows the same trend. This behavior can also be noted when considering the change in side force coefficient. When regarding the deltas in drag force coefficient the superposition values do not match and additionally the trend of the two curves diverge.

The deltas of moment coefficients for roll, pitch and yaw no match very well for the entire angle of attach range and even depict the nonlinear behavior at high angles of attack.

Hence it can be shown that the delta of the forces coefficients for deflection combinations depicted in **Figure 17** cannot be added up in order to represent the overall behavior of the configuration throughout the entire angle of attack range tested. However it seems that the moment behavior can be represented when adding up the delta changes for full span deflection left and full span deflection right.

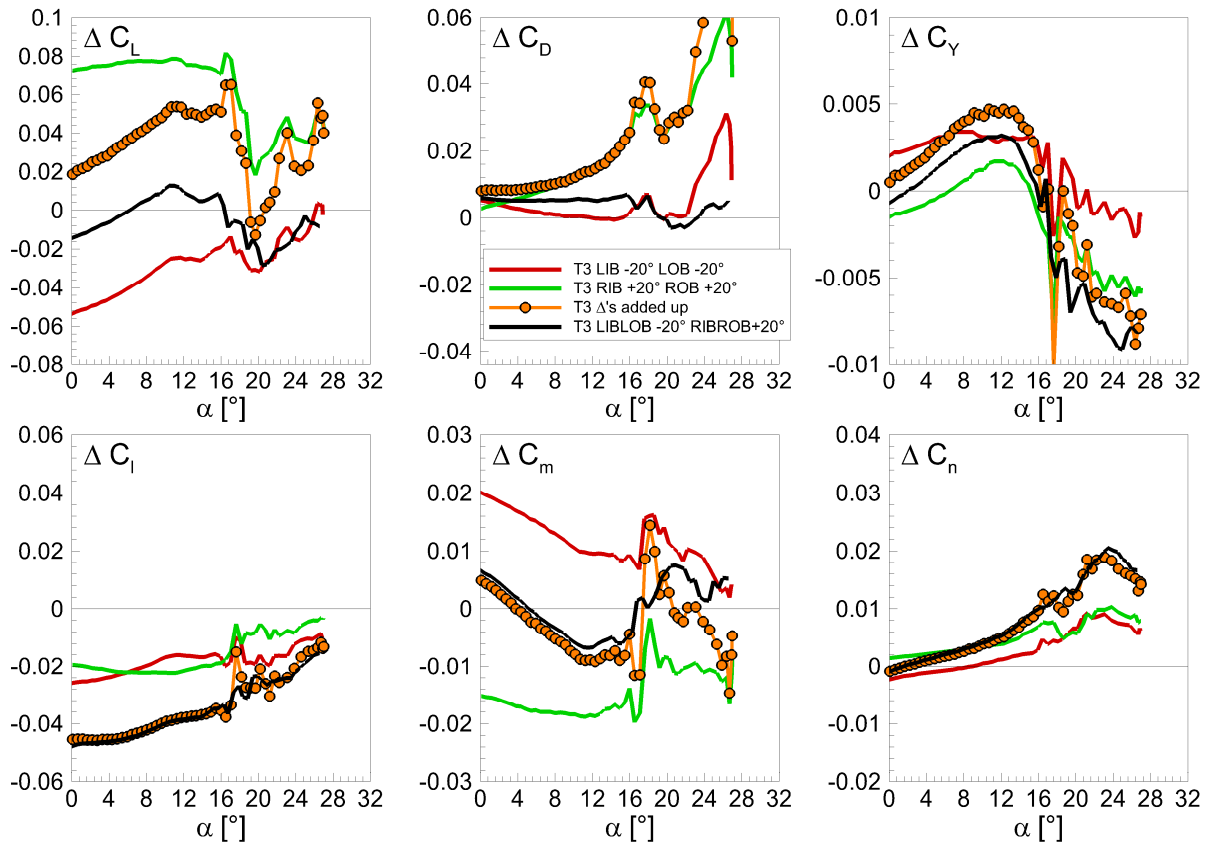


Figure 18 Superposition Effects – full span control surface deflection.

I. Utilization of Experimental Data

During the experimental campaigns T0, T1, T2 and T3 a large amount of static and dynamic data for this generic lambda wing configuration at low speeds was collected. A discussion of the results for the dynamic data can be found in Vicroy et al.²⁹ Further experimental data at high speeds have also been collected; further information can be found in Irving et al.¹⁷ The experimental data will be used to fill an aerodynamic database in order to create a flight mechanics model for further Stability and Control analyses. Results from the test campaigns serve also as basis for a common static test case matrix for CFD in Schuette et al.¹⁵ and Zimper et al.¹⁸ All these research aspects just mentioned will be conducted with the NATO STO AVT-201 international research group and a possible follow on group AVT-239.

Conclusion

Two identical generic UCAV model configurations with different control surfaces have been experimentally investigated. Low speed static wind tunnel tests have been undertaken to evaluate the effectiveness of different control surfaces and control surface settings. The experimental results are used to establish a common CFD test matrix for the NATO STO Task Group AVT-201 for computer code validation and to assess the capability to predict the complex vortical flow and aerodynamic Stability and Control characteristics of configurations with highly swept leading edges and vortex dominated flow field. This work shows that the repeatability and reproducibility between the different experimental investigations is satisfactory and hence all experimental investigations of the configuration can be included into further Stability and Control analysis studies. Deflection angles up to $\eta = 10^\circ$ do only have a small influence on the forces and moments. Hence it was decided to use a minimum deflection angle of $\eta = 20^\circ$ for further experimental and numerical investigations. The control surface depth was chosen to be at 75% of C_{ref} . It has been confirmed that the control surface deflection has a distinct effect on the moments and only small effects on the forces. Also an inboard deflected control surface has a considerably larger effect on the flow than a control surface deflected on the outer wing area. It was shown that the forces and moment coefficients for single

deflections can be added up in order to represent the overall behavior of the configuration throughout the entire angle of attack range tested. This finding has a great influence on the creation of possible stability and control databases for this kind of configurations, data bases can be filled with extra points without extra measurements. For the cases of more multiple control surface combinations, the effect due to control surface interactions is too large and hence the effects of the individual parts cannot be added up to reproduce the aerodynamic behavior.

Acknowledgments

The authors would like to thank the whole team from the DNW-NWB wind tunnel in Braunschweig establishing the data with the DLR-F19 model configuration. Furthermore they would like to thank all the members of NATO STO AVT-201 Task Group on “Extended Assessment of Stability and Control Prediction Methods for NATO Air Vehicles” for the very fruitful discussions and cooperation work.

The authors from DLR would like to thank the German Ministry of Defense and The Federal Office of Bundeswehr Equipment, Information Technology and In-Service Support (BAAINBw) for their support for the military research at DLR and the support to attend the NATO STO/AVT Task Group meetings.

References

- ¹ Huebner, A.-R.; Vicroy, D.D.; Schuette, A.; and Huber, K. C.: “*Experimental and Numerical Investigation of Dynamic Derivatives of an UCAV Configuration*,” RTO / AVT-189/RSM-028 Specialists Meeting, October 12-14, 2011.
- ² Vicroy, D.D.; Huber, K.C.; Loeser, T.; and Rohlf, D.: “*Low-speed Dynamic Wind Tunnel Test Analysis of a Generic 53° Swept UCAV Configuration with Controls*,” AIAA-2014-2003, 32nd AIAA Applied Aerodynamics Conference, Atlanta, GA, June 16-20, 2014.
- ³ Rein, M.; Irving, J.; Rigby, G., and Birch, T.: “*High speed static experimental investigations on a generic UCAV to estimate control device effectiveness and S&C capabilities*,” AIAA-2014-2004, 32nd AIAA Applied Aerodynamics Conference, Atlanta, GA, June 16-20, 2014.
- ⁴ Cummings, R.M.; and Schuette, A.: “*Integrated Computational/Experimental Approach to Unmanned Combat Air Vehicle Stability and Control Estimation*,” Journal of Aircraft, Vol. 49, No. 6 (2012), pp. 1542-1557. DOI: 10.2514/1.C031430.
- ⁵ Cummings, R.M.; Schuette, A. et al.: *Summary Report of the NATO RTO/AVT-161 Task Group on “Assessment of Stability and Control Prediction Methods for NATO Air and Sea Vehicles*,” RTO-TR-AVT-161 AC/323 (AVT-161) TP/440, Sept. 2012.
- ⁶ Liersch, C. and Huber, K.C.: “*Conceptual control surface design and aerodynamic analyses of a generic UCAV Configuration*,” AIAA-2014-2001, 32nd AIAA Applied Aerodynamics Conference, Atlanta, GA, June 16-20, 2014.
- ⁷ Cummings, R.M.; Schuette, A.; and Huebner, A.-R.: “*Overview of Stability and Control Estimation Methods from NATO STO Task Group AVT-201*” 51st AIAA Aerospace Sciences Meeting including the New Horizons Forum and Aerospace Exposition, 2013, DOI: 10.2514/6.2013-968.
- ⁸ Loeser, T.; A.; Vicroy, D., and Schuette, A.: “*SACCON Static Wind Tunnel Tests at DNW-NWB and 14’x22’ NASA LaRC*,” AIAA- 2010-4393, 28th AIAA Applied Aerodynamics Conference, Chicago, IL, June 28 – July 1, 2010.
- ⁹ Vicroy, D.D.; Loeser, Thomas D., and Schuette A.: “*Static and Forced-Oscillation Tests of a Generic Unmanned Combat Air Vehicle*,” Journal of Aircraft, Vol. 49, No. 6 (2012), pp. 1558-1583. DOI:10.2514/1.C031501.
- ¹⁰ Schuette, A.; Hummel, D., and Hitzel, S.M.: “*Flow Physics Analyses of a Generic Unmanned Combat Aerial Vehicle Configuration*,” Journal of Aircraft, Vol. 49, No. 6 (2012), pp. 1638-1651, DOI: 10.2514/1.C031386.
- ¹¹ Huber, K.C.: “*Numerical Investigation of the Aerodynamic Properties of a Flying Wing Configuration*,” DLR internal Report IB 124-2012/4 (2010).
- ¹² Website of the German Dutch Wind Tunnels: <http://www.dnw.aero/wind-tunnels/nwb.aspx> [14th May 2014].
- ¹³ Bergmann, A.; Huebner, A.-R., and Loeser, T.: “*Experimental and numerical research on the aerodynamics of unsteady moving aircraft*,” Progress in Aerospace Sciences vol. 44 issue 2 February, 2008. p. 121-137.

¹⁴ Bergmann, A.: *The Model Positioning Mechanism of DNW-NWB based on a new parallel kinematic*, Open Technology Forum, Aerospace Testing Expo, Hamburg, April 2005.

¹⁵ Schütte, A.; Huber, K.C., and Boelens, O.J.: "*Static and dynamic numerical simulations of a generic UCAV configuration with and without control devices*", "AIAA-2014-2132, 32nd AIAA Applied Aerodynamics Conference, Atlanta, GA, June 16-20, 2014.

¹⁶ Huber, K.C.; Schuette, A., and Rein, M.: "*Numerical Investigation of the Aerodynamic Properties of a Flying Wing Configuration*", "AIAA 2012-3325, 30th AIAA Applied Aerodynamics Conference, New Orleans, LA, June 25-28, 2012.

¹⁷ Rein, M.; Irving, J.; Rigby, G., and Birch, T.: "*High speed static experimental investigations on a generic UCAV to estimate control device effectiveness and S&C capabilities*", "AIAA-2014-2004, 32nd AIAA Applied Aerodynamics Conference, Atlanta, GA, June 16-20, 2014.

¹⁸ Zimper, D., and Rein, M.: "*Experimental and numerical analysis of the transonic vortical flow over a generic lambda wing configuration*", "AIAA-2014-2005, 32nd AIAA Applied Aerodynamics Conference, Atlanta, GA, June 16-20, 2014.